TABLE I Lattice constants of AlN, AlN^{δ} and δ-AlN

	a-axis (Å)	*c*-axis (Å)
AlN [8]	3.114	4.986
AlN^{δ} [7]	3.079	5.30
δ-AlN (present)	3.07 ± 0.01	5.2 ± 0.1

diffuse phase, named AlN^{δ}, has a wurtzite structure like AlN, the lattice constants being elongated in the *c*-direction and shrunk in the *a*-directions compared with AlN crystal. The lattice constants obtained for δ-AlN are tabulated with those of AlN^{δ} and AlN in Table I. These results suggest that δ-AlN (the present film) may be the same as AlN^{δ} (Jack's result). The existence of oxygen in δ-AlN film could not be confirmed. Considering the chemical activities of Si and Al to oxygen, however, it is plausible to consider that oxygen was taken into the film from residual gas and that δ-AlN film was constituted with the Al–Si–N–O system.

The definite splitting of the diffraction spots of AlN and δ-AlN in Fig. 1 suggests that Si atoms occupy the substitutional site rather than the intersitial site in AlN. It is naturally considered from their ionic radii that the O atom substitutes for N. It seems difficult, however, to decide whether Si substitutes for Al or N.

In conclusion, we have confirmed that Si can be doped rather easily into AlN crystal by using a d.c. glow discharge method. The formation mechanism of nitride film by this method is considered to be as follows; the surface of AlN film reacts with active nitrogen created by the glow discharge while the cathode materials (Si) are sputtered onto substrate. Then the AlN film including Si grows on the Al film. This suggests that another metal impurity may be doped into AlN by this method, which would be appropriate for searching the materials dopable into AlN film. The δ-AlN film is an electrically good insulator like AlN film, and detailed experiments on electrical properties are now being carried out with metal–insulator–metal type diodes.

References

1. T. L. CHU, D. W. ING and A. J. NOREIKA, *Solid State Electron.* **10** (1967) 1023.
2. H. M. MANASEVIT, F. M. ERDMANN and W. I. SIMPSON, *J. Electrochem. Soc.* **118** (1971) 1864.
3. A. J. SHUSKAS, T. M. REEDER and E. L. PARADIS. *Appl. Phys. Letters* **24** (1974) 155.
4. S. YOSHIDA, S. MISAWA and A. ITOH, *ibid* **26** (1975) 462.
5. Y. UEMURA, K. TANAKA and M. IWATA, *Thin Solid Films* **20** (1974) 11.
6. Y. UEMURA and M. IWATA, *J. Crystal Growth* **29** (1975) 127.
7. K. H. JACK, *J. Mater. Sci.* **11** (1976) 1135.
8. ASTM X-ray Powder Data File No. 8-262.

Received 16 March
and accepted 28 April 1977.

YOICHIRO UEMURA
MINORU IWATA
National Institute for Researches in Inorganic Materials, Kurakake, Sakura-Mura, Ibaraki-Ken, Japan

On carbide cracking as a source of acoustic emission in steel

Although Acoustic Emission (AE) detection is being widely used as a non-destructive-testing technique, especially in flaw location, the microscopic sources of emission are not generally well understood. For example, in steels of a ferrite/cementite microstructure the role of carbide cracking in generating detectable emission is unclear [1–4]. The present study was carried out to help clarify this particular problem.

Uniaxial tensile tests, using specimens of dimensions shown in Fig. 1a, were carried out on a spherodized steel of composition:

C	Mn	Si	P	S
1.10	0.17	0.16	0.009	0.009
Cr	Cu	Ni	Sn	Al(tot)
0.05	0.15	0.06	0.02	0.03

After machining, the specimens were vacuum heat-treated at 680° C for 3 h followed by furnace cooling. The mechanical testing was carried out at room temperature in an Instron floor model tensile-testing machine at a cross-head displacement rate of 2 mm min^{-1}. Simultaneous AE measurements were made on all specimens using a

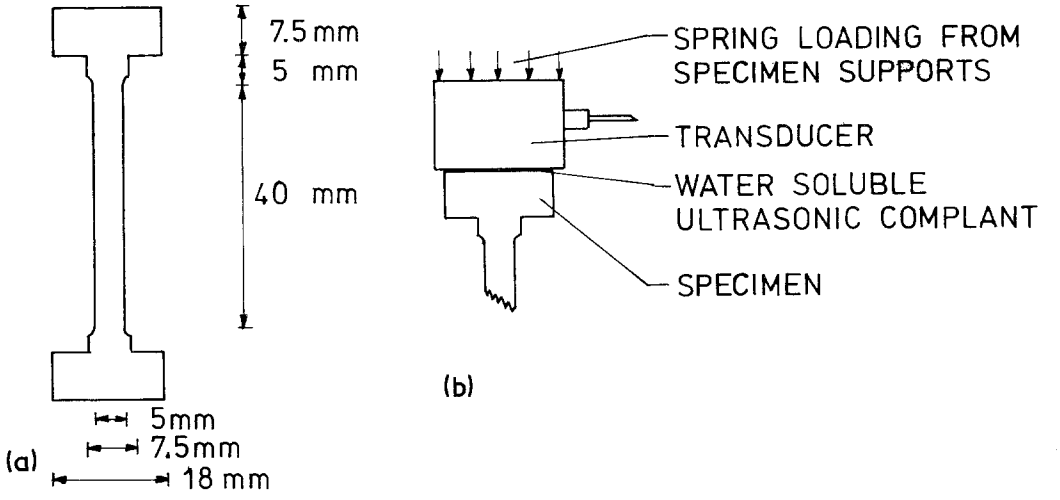

Figure 1 (a) Dimensions of test specimen. (b) Connection of transducer to specimen head.

transducer* clamped on the specimen head, Fig. 1b. After pre-amplification signals were recorded on a modified videotape recorder and replayed subsequently for analysis. The signals were analysed in an event count mode, using a 0.5 msec counter dead-time.

Specimens were extended to various uniform strains, unloaded, sectioned longitudinally, polished and etched in 4% Nital. The cumulative carbide crack density (mm^{-2}) was followed as a function of strain using optical microscopy and Scanning Electron Microscopy† (SEM). A magnification of 650 was used for optical measurements and 3000 for the electron microscopy. Eight areas of approximately 10^4 μm^2 per field were investigated optically for each specimen, while one such area per specimen was investigated by SEM.

The cumulative carbide crack density is shown as a function of strain in Fig. 2. Optical and SEM photographs of a typical specimen microstructure are shown in Fig. 3. The three parameters, load on specimen, AE event count rate and AE cumulative event count, are shown in Fig. 4 for a specimen strained to failure.

SEM was used in conjunction with optical microscopy because of the higher resolution available. The similarity between the two sets of data indicates their reliability. An approximately linear increase of crack density (mm^{-2}) with strain is apparent up to a strain of $\epsilon = 20\%$. This is in agreement with the work of Gurland [5].

*Dunegan/Endevco D9203.

†JEOL 100 C (plus scanning attachment).

With reference to Fig. 4 it can be seen that most of the emission is generated during the first 8% strain. Much emission is generated during Lüders deformation. A second smaller peak is located between $\epsilon = 2\%$ and $\epsilon = 5\%$, with a rapid fall-off in emission rate thereafter. Considering the number of carbide cracks mm^{-3} to be proportional to the number mm^{-2}, then Fig. 4 may be compared with Fig. 2 if it is assumed that one AE event is generated for each carbide fracture. Thus Fig. 2 implies a constant carbide cracking rate (mm^{-3}) as a function of strain, while Fig. 4b shows a rapid decrease in the emission event count rate with

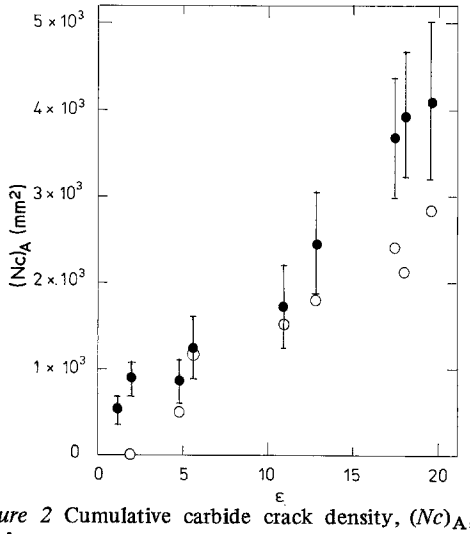

Figure 2 Cumulative carbide crack density, $(Nc)_A$, per mm^2 as a function of strain, ϵ. • Optical microscopy measurements. ○ Scanning electron microscopy measurements.

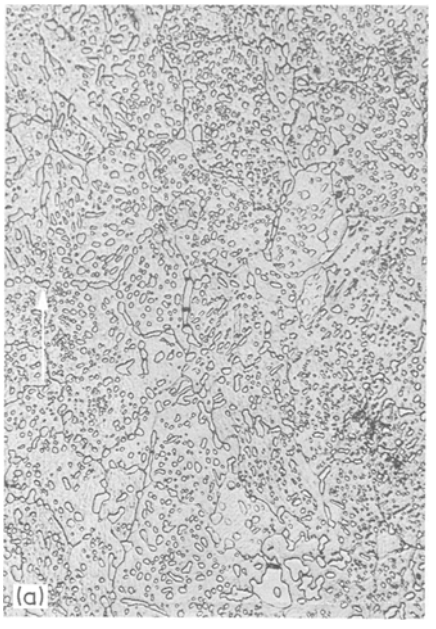

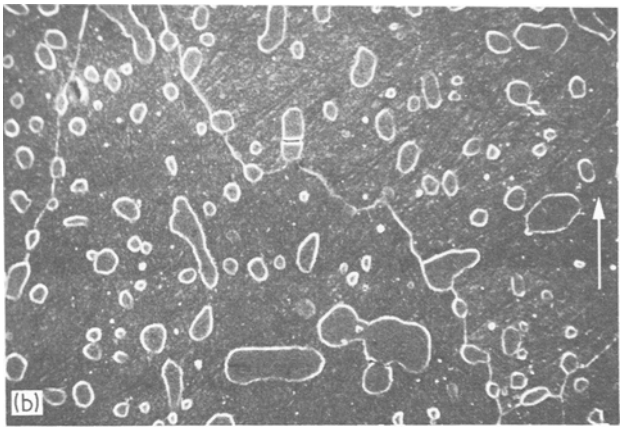

Figure 3 Microstructure of specimen deformed in uniaxial tension. (a) Optical micrograph (× 800). (b) Scanning Electron Micrograph (× 3000). Tensile axis as shown by arrow on micrographs.

strain. The absence of a correlation between the two functions indicates that carbide cracking is not responsible for the AE detected.

A further point of interest arises from this investigation; the relevance of this type of study to the analysis of emission from structural steels with ferrite/pearlite microstructures. Although no experiments combining AE and carbide cracking as a function of strain have been published, it is possible to correlate the data from published investigations where these parameters have been investigated independently. The cracking of carbides (in the form of isolated platelets and in pearlite colonies) has been followed in low-carbon steels and irons as a function of strain at room temperature by Barnby and Johnson, Clausing, Lindley *et al.*, Brindley, and Rosenfield *et al.* [6–10]. The results show a general increase of cumulative crack density with strain. However, AE investigations of low-carbon steels by Ingham *et al.*, Ono *et al.*, and Dunegan and Green [2, 3, 11] all show that, as in the present case, emission rates are very high during Lüders deformation and tend to fall off rapidly with strain after 4 to 5% deformation. A comparison between the two sets of data thus indicates that emission sources, other than carbide cracking, can be predominant in these materials. Researches at present being conducted by the author point to similar conclusions.

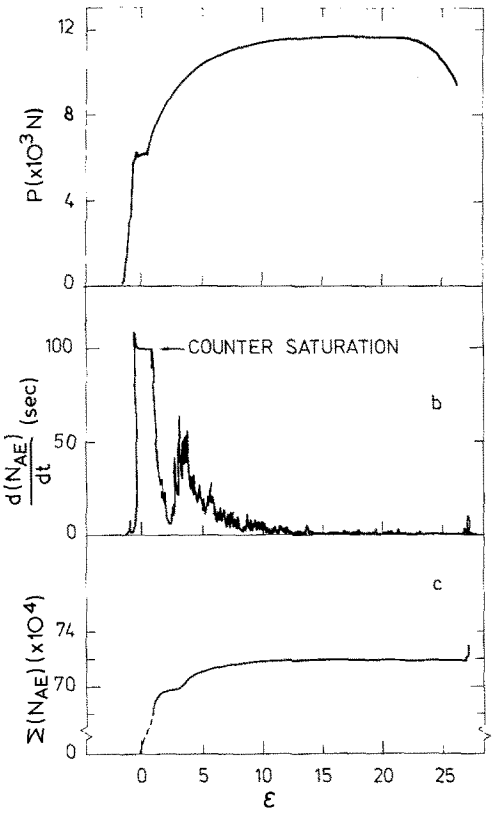

Figure 4 (a) Load, P, on specimen as a function of specimen strain, ϵ. (b) Acoustic emission event count rate, $d(N_{AE})/dt$, and (c) Cumulative acoustic emission event count, $\Sigma(N_{AE})$, as a function of specimen strain, ϵ.

As the above discussion is limited to uniaxial tensile tests, it would be premature to reach any general conclusions about carbide cracking in pearlite as an emission source in all deformation situations. For uniaxial tensile stress conditions, Miller and Smith [12] have proposed a crack propagation mechanism whereby the cracking of individual carbide plates extends progressively throughout a pearlite colony, via slip in the interplate ferrite. However, if such a process, from the AE standpoint, occurs slowly the unit emission source will be the fracture of individual carbide lamellae. On the other hand, the general stress field around a colony could affect such a deformation process. For example, in crack propagation tests, stress triaxially in the crack tip region may promote the pearlite to fail in such a way that many individual carbide plates fracture simultaneously. Under these conditions the unit emission process would not be the same as that described above. Thus the emission characteristics of one particular microstructural feature may well be different in different stress field configurations.

References

1. D. BIRCHON, *Brit. J. NDT* 18 (1976) 66.
2. T. INGHAM, A. L. STOTT and A. COWAN, *Int. J. Press, Ves. Piping* 2 (1974) 31.
3. K. ONO, G. HUANG and H. HATANO, Eighth World Conference on Non-Destructive Testing, Cannes, France, 6–11 November 1976.
4. J. HOLT and I. G. PALMER, Proceedings of the Symposium of the German Metallurgical Society. Acoustic Emission, Munich, April 1974, p. 24.
5. J. GURLAND, *Acta Met.* 20 (1972) 735.
6. J. T. BARNBY and M. R. JOHNSON, *Met. Sci. J.* 3 (1969) 155.
7. D. P. CLAUSING, *Trans. A.S.M.* 60 (1967) 504.
8. T. C. LINDLEY, G. OATES and C. E. RICHARDS, *Acta Met.* 18 (1970) 1127.
9. B. J. BRINDLEY, *Acta Met.* 18 (1970) 325.
10. A. R. ROSENFIELD, G. T. HAHN and J. E. EMBURY, *Met. Trans.* 3 (1972) 2799.
11. H. L. DUNEGAN and A. T. GREEN, ASTM. STP. 505; (1972) 100.
12. L. E. MILLER and G. C. SMITH, *J. Iron Steel Inst.* 208 (1970) 998.

Received 16 March
and accepted 28 April 1977

W. E. SWINDLEHURST
Metallurgy Department
Risφ National Laboratory
4000 Roskilde, Denmark

Prediction of thermal fatigue life of ceramics

Crack growth in one cycle of thermal stress can not be given easily due to the difficulty in knowing the precise thermal stress distribution. This seems to make it difficult to relate the results of short-term tests to the fatigue life in practice. However, consideration of the fact that the fatigue life is approximated by the duration in which the crack length reaches a certain critical value, beyond which the growth becomes relatively rapid, may make the prediction easy.

The slow crack growth can be described by

$$\frac{da}{dt} = AK_I^n \qquad (1)$$

where a, t, K_I, A and n stand for crack length, time, stress intensity factor and material constant, respectively [1]. K_I is, also, expressed by

$$K_I = Ya^{1/2}\sigma \qquad (2)$$

where Y and σ stand for geometrical factor and applied stress, respectively [2]. Substitution of Equation 2 into Equation 1 gives,

$$\frac{da}{dt} = AY^n a^{n/2}\sigma^n \qquad (3)$$

σ, in general, consists of mechanical stress, σ_M, and thermal one, σ_T. When thermal fatigue limits the life of a ceramics, σ_M can be neglected and

$$\sigma \approx \sigma_T. \qquad (4)$$

Under thermal stress, generally, the stress distribution and the type of the stress change with the crack length as well as time, depending on the shape of the ceramic articles and heating or cooling process. Thus, in general, Y and σ depend on the